L. Lens*, A. Yakushev, Ch. E. Düllmann, M. Asai, J. Ballof, M. Block, H. M. David, J. Despotopulos, A. Di Nitto, K. Eberhardt, J. Even, M. Götz, S. Götz, H. Haba, L. Harkness-Brennan, F. P. Heßberger, R.-D.Herzberg, J. Hoffmann, A. Hübner, E. Jäger, D. Judson, J. Khuyagbaatar, B. Kindler, Y. Komori, J. Konki, J. V. Kratz, J. Krier, N. Kurz, M. Laatiaoui, S. Lahiri, B. Lommel, M. Maiti, A. K. Mistry, C. Mokry, K. Moody, Y. Nagame, J. P. Omtvedt, P. Papadakis, V. Pershina, J. Runke, M. Schädel, P. Scharrer, T. Sato, D. Shaughnessy, B. Schausten, P. Thörle-Pospiech, N. Trautmann, K. Tsukada, J. Uusitalo, A. Ward, M. Wegrzecki, N. Wiehl, and V. Yakusheva

Online chemical adsorption studies of Hg, Tl, and Pb on SiO$_2$ and Au surfaces in preparation for chemical investigations on Cn, Nh, and Fl at TASCA

...

*Corresponding author: L. Lens, Institut für Kernchemie, Johannes Gutenberg University, 55122 Mainz, Germany; and GSI Helmholtzzentrum für Schwerionenforschung, 64291 Darmstadt, Germany

A. Yakushev, F. P. Heßberger, J. Khuyagbaatar, A. K. Mistry, V. Yakusheva, GSI Helmholtzzentrum für Schwerionenforschung, 64291 Darmstadt, Germany, and Helmholtz-Institut Mainz, 55099 Mainz, Germany

Ch. E. Düllmann, M. Block, M. Götz, S. Götz, P. Scharrer, Institut für Kernchemie, Johannes Gutenberg University, 55122 Mainz, Germany; and GSI Helmholtzzentrum für Schwerionenforschung, 64291 Darmstadt, Germany; and Helmholtz-Institut Mainz, 55099 Mainz, Germany

M. Asai, Y. Nagame, T. Sato, K. Tsukada, Japan Atomic Energy Agency, 319-1195 Tokai-mura, Naka-gun, Ibaraki, Japan

J. Ballof, Institut für Kernchemie, Johannes Gutenberg University, 55122 Mainz, Germany; and GSI Helmholtzzentrum für Schwerionenforschung, 64291 Darmstadt, Germany, and present address: Section Isolde, Cern, 1211 Geneva, Switzerland

H. M. David, J. Hoffmann, A. Hübner, E. Jäger, B. Kindler, J. Krier, N. Kurz, B. Lommel, V. Pershina, B. Schausten, GSI Helmholtzzentrum für Schwerionenforschung, 64291 Darmstadt, Germany

Abstract: Online gas-solid adsorption studies with single-atom quantities of Hg, Tl, and Pb, the lighter homologs of the SuperHeavy Elements (SHE) copernicium (Cn, Z=112), nihonium (Nh, Z=113), and flerovium (Fl, Z=114), were carried out using short-lived radioisotopes. The interaction with Au and SiO₂ surfaces was studied and the overall chemical yield was determined. Suitable radioisotopes were produced in fusion-evaporation reactions, isolated in the gas-filled recoil separator TASCA, and flushed rapidly to an adjacent setup of two gas chromatography detector arrays covered with SiO₂ (first array) and Au (second array). While Tl and Pb adsorbed on the SiO₂ surface, Hg interacts only weakly and reached the Au-covered array. Our results contribute to elucidating the influence of relativistic

J. Despotopulos, K. Moody, D. Shaughnessy, Lawrence Livermore National Laboratory, Livermore, CA 94551, USA

A. Di Nitto, J. Runke, Institut für Kernchemie, Johannes Gutenberg University, 55122 Mainz, Germany; and GSI Helmholtzzentrum für Schwerionenforschung, 64291 Darmstadt, Germany

K. Eberhardt, C. Mokry, P. Thörle-Pospiech, N. Wiehl, Institut für Kernchemie, Johannes Gutenberg University, 55122 Mainz, Germany; and Helmholtz-Institut Mainz, 55099 Mainz, Germany

H. Haba, Y. Komori, Hirosawa, Wako, Saitama 351-0198, Japan

L. Harkness-Brennan, R.-D.Herzberg, D. Judson, A. Ward, Department of Physics, University of Liverpool, L69 7ZE Liverpool, U.K.

P. Papadakis, J. Uusitalo, Department of Physics, University of Jyväskylä, 40014 Jyväskylä, Finland

J. V. Kratz, N. Trautmann, Institut für Kernchemie, Johannes Gutenberg University, 55122 Mainz, Germany

M. Laatiaoui, GSI Helmholtzzentrum für Schwerionenforschung, 64291 Darmstadt, Germany, and Helmholtz-Institut Mainz, 55099 Mainz, Germany, present address: Institute for Nuclear and Radiation Physics, KU Leuven, 3001 Leuven, Belgium

S. Lahiri, Chemical Sciences Division, Saha Institute of Nuclear Physics, 700064 Kolkata, India

M. Maiti, Department of Physics, Indian Institute of Technology Roorkee, 247667 Uttarakhand, India

J. P. Omtvedt, Department of Chemistry, University of Oslo, 0315 Oslo, Norway

M. Schädel, GSI Helmholtzzentrum für Schwerionenforschung, 64291 Darmstadt, Germany, and Japan Atomic Energy Agency, 319-1195 Tokai-mura, Naka-gun, Ibaraki, Japan

M. Wegrzecki, Institute of Electron Technology, 02-668 Warsaw, Poland

J. Even, Institut für Kernchemie, Johannes Gutenberg University, 55122 Mainz, Germany; and GSI Helmholtzzentrum für Schwerionenforschung, 64291 Darmstadt, Germany; and Helmholtz-Institut Mainz, 55099 Mainz, Germany, present address: KVI-Center for Advanced Radiation Technology University of Groningen, 9747 AA Groningen, The Netherlands

J. Konki, Department of Physics, University of Jyväskylä, 40014 Jyväskylä, Finland, present address: Section Isolde, Cern, 1211 Geneva, Switzerland

effects on chemical properties of the heaviest elements by providing experimental data on these lighter homologs.

1 Introduction

Experimental investigations of the chemical and physical properties of Superheavy Elements (SHE), defined as elements with $Z{\geq}104$ [1], represent an exciting and challenging topic in current nuclear chemistry and physics research. To date, the periodic table of the elements includes elements with atomic numbers Z up to 118, see Fig. 1. The discovery of the elements with $Z{=}113$, $Z{=}115$, $Z{=}117$, and $Z{=}118$ was recently confirmed, and they were named nihonium (Nh), moscovium (Mc), tennessine (Ts), and oganesson (Og), respectively [2]. The placement of new elements in the periodic table raises the question of whether they will follow the extrapolation within the chemical group, or whether the influence of relativistic effects (which increase roughly with Z^2 [3, 4, 5]) causes a deviation from periodicities in the group. A suitable approach to study the chemical properties of SHE, is to study their interaction strength with different surfaces, e.g., Au or SiO_2. These results are then compared to those of the lighter homologs in their chemical group [6].

The limitations in investigating the chemical properties of the SHE include their low production rates (with cross sections on the order of nb to pb), and short half-lives (which are mostly less than one minute). Due to the low production rates, the chemical separation of SHE has to be performed on an atom-at-a-time scale and the abundant formation of unwanted byproducts in the nuclear reaction can severely hamper the unambiguous identification of SHE. In order to detect single atoms under almost background-free conditions, chemical techniques are combined with physical preseparation in a recoil separator [7] such as the Trans Actinide Separator and Chemistry Apparatus (TASCA) [8, 9].

A successful technique to study chemical properties of short-lived SHE behind a pre-separator is gas-phase chromatography [6, 10, 11]. Here, the volatile species are transported by a carrier gas through the chromatography column, where the gas-solid interaction takes place. Two different types of chromatographic

Fig. 1: Periodic table of elements (2017). The elements studied in this work (Hg, Tl, and Pb) along with their heavier homologs (Cn, Nh, Fl), as well as Rn are highlighted.

techniques can be used: thermochromatography and isothermal chromatography, both of which can also be combined. In thermochromatography, a negative temperature gradient is applied along a chromatography column, whereas in isothermal chromatography, the temperature along the column is kept constant [12].

The chemical properties of copernicium (Cn, $Z=112$), nihonium (Nh, $Z=113$), and flerovium (Fl, $Z=114$) have recently been investigated in experimental and theoretical studies. Cn and Fl are expected to be inert and volatile atoms due to their closed and quasi-closed electron ground-shell configurations, $6d^{10}7s^2$ and $7s^27p_{1/2}^2$, respectively. This is caused by large relativistic stabilization of the $7s$ and $7p_{1/2}$ valence atomic orbitals (AOs) and large spin-orbit (SO) splitting of the $7p$ AOs [13, 14, 15, 16, 17]. Nh, on the contrary, is expected to be rather reactive due to the availability of one unpaired electron in the ground state configuration $7s^27p_{1/2}$ [18, 19, 20, 21, 22]. However, the strong relativistic contraction and stabilization of the $7s$ and $7p_{1/2}$ AOs and the large SO splitting are also expected to significantly reduce its reactivity when comparing to that of Tl, such that its interaction strength with surfaces might be expected to be reduced compared to Tl.

Gas-phase thermochromatography experiments with chromatography columns formed by Au-covered detectors showed that Cn adsorbs on the Au surface at temperatures below 0 °C [23]. Despite being a very volatile element, a metal-bond formation with Au, which is much weaker than for Hg on Au, was found. Copernicium conforms well to the trend in group 12 of the periodic table [24].

Experiments on the adsorption properties of Fl using a similar experimental technique turned out to be contradictive. In earlier experiments, which did not use a pre-separator [16], Fl decay was observed at low temperatures of the Au covered detectors in the chromatography columns. Based on this result, a high volatility and low reactivity for Fl was inferred. However, subsequent experiments, using a similar setup, but with a pre-separator, have shown a much lower volatility of Fl, which was interpreted as an indication for a metal-metal bond formation [25].

A first attempt to study chemical properties of Nh was reported in ref. [26]. Since no pre-separator was used in this experiment, the background in the detection area could affect the identification of the ^{284}Nh events. Based on the obtained results, the authors of [26] concluded that Nh has a high reactivity towards Au. No information on the chemical form of Nh (atomic vs. NhOH) was given. An attempt to investigate Nh under reduced background conditions was performed [27]. No decay chains originating from Nh isotopes were observed in this study. A common interpretation to explain the observed results were given in [27] for both experiments [26, 27]. This suggested the formation of NhOH in the first study, while the formation of elemental Nh, which did not reach the detection system, was proposed for the second study.

Due to limited statistics and high background in experiments without pre-separator, further advanced experimental studies with a pre-separator appear essential to clarify the chemical properties of Nh and Fl. For this, the experimental setup has to be optimized and the sensitivity should be increased. The optimization of the chemical procedure (transport efficiency, flush-out time, and chemical separation in the detection setup) was performed with short-lived isotopes of the lighter homologs, Hg, Tl, and Pb. They could be produced with significantly higher rates in fusion reactions and then pre-separated by TASCA.

Several offline experiments with the isotopes of Tl and Pb were performed to determine the adsorption behavior on Au- and SiO_2-covered detector surfaces [28, 29, 30]. With Hg, offline as well as also online experiments were performed [31, 23]. It was shown, that Hg adsorbs only very weakly on SiO_2, but interacts strongly with Au at room temperature (21 °C). On the contrary, Tl as well as Pb, interact strongly with both surfaces, and adsorb on both of them at room temperature. In the investigations of Tl, it was observed that the chemical form of Tl is extremely sensitive to trace amounts of oxygen and water. Even hydroxyl groups located on the SiO_2 surface were observed to oxidize Tl [29]. On a SiO_2 surface, Tl forms TlOH. On a Au surface, two Tl species could be observed, and were interpreted to be atomic Tl as well as TlOH. The first successful online isothermal vacuum chromatography experiment on the interaction of Tl with SiO_2 surfaces was reported in ref. [32] and was in modest agreement with results from the earlier offline experiments.

Since studies of the chemical properties of SHE should be performed online, it is crucial to investigate their homologs online in the same experimental setup. Hence, we report on *online* chemical adsorption studies of Pb and Hg on SiO$_2$ and Au surfaces, in the same experimental setup as used for the Cn, Nh, and Fl studies. Furthermore, we report on online gas-phase chromatography experiments with Tl. The results of the present investigations for Hg, Tl, and Pb will be invaluable for the evaluation of studies on the chemical behavior of their heavier homologs, Cn, Nh, and Fl.

2 Experimental setup and methods

2.1 Experimental setup

The experiments were performed at GSI in Darmstadt, Germany. A combination of the gas-filled recoil pre-separator TASCA and the gas chromatography and detection system COMPACT (Cyro-Online Multi detector for Physics And Chemistry of Transactinides) [33], was used, as shown in Fig. 2.
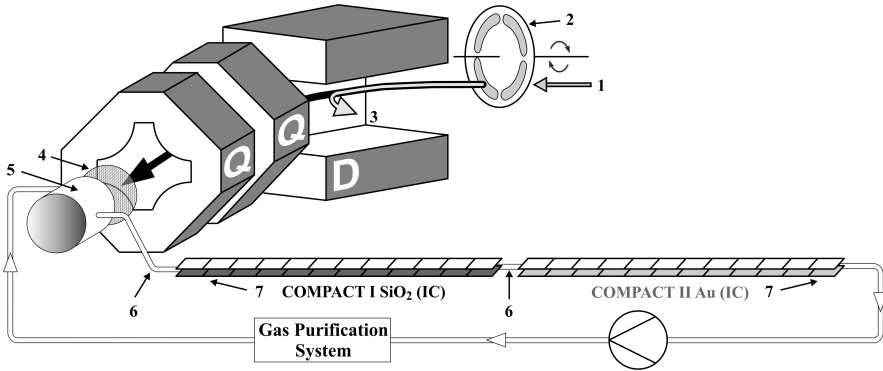
Fig. 2: Schematic drawing of the TASCA COMPACT arrangement used for gas chromatographic investigations of $^{181-186}$Hg, $^{183-185}$Tl, and $^{185-187}$Pb on SiO_2 and Au surfaces. The primary beam (1) passed through a rotating target (2) assembly. The separator TASCA consists of one dipole (D) magnet, where unwanted nuclear reaction products and unreacted primary beam (3) are separated from evaporation residues subsequently and focused by means of two quadrupole (Q) magnets. At the exit of TASCA a vacuum window (4) separated the low-pressure region in TASCA from the high-pressure region in the recoil transfer chamber (RTC) (5). After passing the window, Hg, Tl, and Pb ions were thermalized in the gas inside the RTC and were transported with a carrier gas through Polytetrafluoroethlylene (PTFE) capillaries (6) into a series of two COMPACT detector arrays (7). To purify the carrier gas, a gas purification system was installed, through which the carrier gas was pumped in a loop.

A beam of accelerated ^{50}Ti^{8+} ions was provided by the UNIversal Linear ACelerator (UNILAC) in an energy range of 5 to 6 MeV/nucleon. The UNILAC provides pulsed beams with a length of about 5 ms. Typical repetition rates were 43 to 45 Hz, and 5 Hz, respectively. In total, a projectile dose of $1.8 \cdot 10^{14}$ *(0.2)* was collected for Hg studies, $4.4 \cdot 10^{15}$ *(0.4)* for Tl, and $4.9 \cdot 10^{15}$ *(0.5)* for studies with Pb. The uncertainty of the beam dose is around 10% [34]. The projectiles passed through a backing foil of carbon ($\approx$40 to 50 $\mu g/cm^2$) before entering the ^{140}CeF$_3$, ^{141}PrF$_3$, or ^{142}NdF$_3$ target, enriched to 99.98%. Four segments of 6 cm^2 area each contained target material ($\approx$400 $\mu g/cm^2$), and were mounted on a rotating wheel with 10 cm diameter. The target wheel rotated synchronously with the macro structure of the primary beam to distribute each beam pulse evenly over one target segment [35]. In complete fusion reactions, ^{190}Hg*, ^{191}Tl*, and ^{192}Pb* compound nuclei were formed at excitation energies of several tens of MeV. After de-excitation, by evaporation of neutrons, a fraction of the resulting isotopes of Hg, Pb, and Tl recoiled from the target into TASCA, which was operated in High Transmission Mode (HTM) [36]. Tab. 1, shows the

projectile-target combinations used to produce isotopes of Hg, Tl, and Pb for the chemical adsorption studies, whereas Tab. 2, shows the combinations used to produce isotopes of Hg and Pb to determine the overall chemical yield from RTC to COMPACT setup.

For each projectile- target combination only the most intense production channels according to HIVAP calculations [37] are listed. In addition decay modes of primary products and the relative α-decay probability (b$_\alpha$) and most intense α-lines (E$_\alpha$) are included. The information presented in Tab. 1 are of importance for the data analysis, see section results and discussion (section 3).

Table 1: ^{50}Ti induced reactions for Hg, Tl, and Pb isotopes production to determine their chemical interaction strengths with the Au and SiO$_2$ surface. The beam energy in the center of the target considered in HIVAP calculations was 277-284 MeV. Calculated cross-sections and decay properties [38, 39], relevant for the data analysis are given.

Reaction	Evaporation channel	Primary products	σ [mb]	Decay mode	b_α [%]	E_α [MeV]	$T_{1/2}$ [s]	Decay products
^{50}Ti + ^{140}Ce	xn	^{182}Hg	2.50	α EC/β^+	13.80 (2)	5.87	10.80	^{178}Pt ^{182}Au
		^{183}Hg	9.90	α EC/β^+	11.70 (20)	5.90	8.80	^{179}Pt ^{183}Au
		^{184}Hg	2.70	α EC/β^+	1.11 (6)	5.54	30.60	^{180}Pt ^{184}Au
^{50}Ti + ^{142}Nd	xn	^{185}Pb	0.31	α EC/β^+	≤100	6.41	4.10	^{181}Hg ^{185}Tl
		^{186}Pb	0.76	α EC/β^+	40.00 (8)	6.33	4.83	^{182}Hg ^{186}Tl
		^{187}Pb	0.08	α EC/β^+	9.50 (20)	6.07	18.30	^{183}Hg ^{187}Tl
^{50}Ti + ^{142}Nd	pxn	^{185}Tl	4.50	α EC/β^+	≤4.00	5.99	1.83	^{181}Au ^{185}Hg
		^{186}Tl	4.10	α EC/β^+	~0.006	5.76	2.90	^{182}Au ^{186}Hg
^{50}Ti + ^{142}Nd	αxn	^{181}Hg	0.01	α EC/β^+	36.00 (4)	6.00	3.60	^{177}Pt ^{181}Au
		^{182}Hg	0.50	α EC/β^+	13.80 (2)	5.87	10.80	^{178}Pt ^{182}Au
		^{183}Hg	2.00	α EC/β^+	11.70 (20)	5.90	8.80	^{179}Pt ^{183}Au
		^{184}Hg	0.80	α EC/β^+	1.11 (6)	5.54	30.60	^{180}Pt ^{184}Au
		^{185}Hg	3.60	α EC/β^+	6.00 (1)	5.65	49.10	^{181}Pt ^{185}Au
^{50}Ti + ^{141}Pr	xn	^{183}Tl	0.30	α EC/β^+	≤0.01	6.34	6.90	^{179}Au ^{183}Hg
		^{184}Tl	2.80	α EC/β^+	2.10 (7)	6.16	11.00	^{180}Au ^{184}Hg
		^{185}Tl	1.60	α EC/β^+	≤4.0	5.99	19.50	^{181}Au ^{185}Hg
^{50}Ti + ^{141}Pr	pxn	^{183}Hg	2.30	α EC/β^+	11.70 (20)	5.90	8.80	^{179}Pt ^{183}Au
		^{184}Hg	11.30	α EC/β^+	1.11(6)	5.54	30.60	^{180}Pt ^{184}Au
		^{185}Hg	3.70	α EC/β^+	6.00(1)	5.65	49.10	^{181}Pt ^{185}Au

Table 2: ^{48}Ca induced reactions for Hg, and Pb isotopes production to determine the overall chemical yield. The beam energy in the center of the target considered in HIVAP calculations was 242-246 MeV. Calculated cross-sections and decay properties [38, 39], relevant for the data analysis are given.

Reaction	Evaporation channel	Primary products	σ [mb]	Decay mode	b_α [%]	E_α [MeV]	$T_{1/2}$ [s]	Decay products
^{48}Ca + ^{142}Nd	*xn*	^{182}Hg	0.001	α EC/β^+	13.80 *(2)*	5.87	10.80	^{178}Pt ^{182}Au
		^{183}Hg	3	α EC/β^+	11.70 *(20)*	5.90	8.80	^{179}Pt ^{183}Au
		^{184}Hg	30	α EC/β^+	1.11 *(6)*	5.54	30.60	^{180}Pt ^{184}Au
^{48}Ca + ^{144}Sm	*xn*	^{185}Pb	0.001	α EC/β^+	$\leq$100	6.41	4.10	^{181}Hg ^{185}Tl
		^{186}Pb	2	α EC/β^+	40.00 *(8)*	6.33	4.83	^{182}Hg ^{186}Tl
		^{187}Pb	4	α EC/β^+	9.50 *(20)*	6.07	18.30	^{183}Hg ^{187}Tl

The primary beam and unwanted nuclear reaction products were deflected by TASCA´s dipole magnet on the beam stop, while Hg, Tl, and Pb ions were guided into the focal plane of the separator. The magnets were set to focus ions with a magnetic rigidity, B·ρ, of 1.58 T·m. At the focal plane of TASCA, they penetrated a Mylar vacuum window (140x40 mm^2 width for Hg and 40x30 mm^2 width for Tl and Pb) of 6 μm thickness, mounted on a 1-mm thick supporting grid of 80% geometrical transparency. The Mylar window was needed to separate the low pressure region (0.8 mbar He gas) in TASCA from the high pressure region (∼1 bar Ar gas) in the Recoil Transfer Chamber (RTC) [40].

Based on calculations using the SRIM code [41, 42] of the kinetic energies and recoil ranges of the EVRs, the Mylar window thickness was selected to provide maximum transmission through the window at minimum remaining recoil range after exiting the window into the gas inside the RTC. This enables the use of a RTC with minimum depth and hence minimized volume, which is beneficial for fast flushing and hence high yield even for short-lived species.

Inside the RTC, Hg, Tl, and Pb isotopes were thermalized in Ar gas (purity: 99.999%), and flushed with a total flow rate of 1.7 to 2.2 L/min into the COMPACT chromatography and detection system. The gas circulated in a loop through a gas purification system. It consisted of several Oxysorb and Hydrosorb cartridges, together with a titanium getter. They were operated in series to minimize oxygen and water contents in the gas. Monitoring of the gas purity was done by constant dew point measurements, as well as frequent gas measurements with a quadrupole mass spectrometer (QMS).

For the investigations on Hg isotopes, a HTM-RTC (56 cm^3) was used. It was constructed from stainless steel, with the interior wall covered with polytetrafluoroethylene (PTFE). At first, Hg isotopes were flushed from the RTC through a 20-cm long PTFE capillary ($\varnothing$ 1 mm) into the first of two COMPACT detector arrays. As the experiment progressed the connection between RTC and COMPACT I, was exchanged by a 4 to 5 cm-long PTFE capillary ($\varnothing$ 4 mm), to reduce the transport time. For Tl and Pb a SIM-RTC (Small Image Mode) (29 cm^3) was used, made from PTFE, allowing for a much shorter (2 to 3 cm-long) PTFE capillary ($\varnothing$ 4 mm) connection between the RTC and COMPACT I.

Each COMPACT detector array consisted of 32 pairs of (1x1) cm^2 large positive-intrinsic-negative (PIN) epitaxial silicon photodiodes. They have an active area of (9.7x9.8) mm^2 and an effective thickness of 150 μm. A gap of 0.6 mm between the top and bottom 32 PIN diode pairs formed a gas channel through each COMPACT detector array. The calculated geometrical efficiencies for detecting an α-particle from atoms present inside a detector array were about 76% respectively [43].

The energy resolution of the Si-detectors when placed in vacuum and irradiated with α particles incoming normal to the detector surface is $\approx$50 keV. When α particles are emitted from species located inside the detector channel, the energy resolution is reduced and low-energy tailing appears. This is due to i) additional energy loss inside the gas in the channel and ii) some particle hitting the surface of the detector under a shallow angle. The first aspect depends on the pressure and composition of the carrier gas, and the second leads to an increased energy loss in the detector dead layer. For measurements using pure Ar gas at 1 bar pressure, the energy resolution was $\approx$200 keV, when pure He was used at 0.3 bar pressure, it was $\approx$100 keV.

Each PIN diode of the COMPACT I detector array was covered with a 35 to 50 nm thick SiO₂ surface, created through the oxidation of Si, while the PIN diodes of the COMPACT II detector were covered by a 30 to 50 nm thick Au layer, deposited by evaporation. Both COMPACT detectors, were operated as isothermal chromatography detectors at room temperature (21 °C). A short PTFE capillary connected the two COMPACT detectors. The COMPACT detectors were calibrated with α particles from the decay of ^{219}Rn and its daughters, emanating from an ^{227}Ac source. The data were processed using full digital electronics. The detector signals were transmitted to flash ADC boards, FEBEX 3A, [44, 45, 46] via preamplifier modules. In order to to extract the energy and time information from the α traces, a pulse shape analysis was performed by onboard FPGA on FEBEX [47]. In addition the signals were saved as digitized traces.

2.2 Monte Carlo Simulations

As discussed in the introduction (section 1), the chemical properties of SHE can be studied by two types of gas phase chromatography techniques: isothermal chromatography and thermochromatography. In thermochromatography a negative temperature gradient is applied along a chromatography column. Depending on the adsorption behavior of the species on the detector surface in the column, their position at the time of decay will vary and so, it is possible to separate different species from each other if their adsorption enthalpies ($-\Delta H_{ads}$) are sufficiently different. In isothermal chromatography, the temperature along the column is kept constant. Depending on the temperature and the $-\Delta H_{ads}$ of the species on the surface of the column, the species travel with different velocities through the column. This retention time can be determined either by injecting a short pulse of the species into the carrier gas and measuring the time at which it emerges through the exit of the column, or by continuously introducing

a short-lived nuclide into the column and measuring the fraction of nuclides decaying in it. Online isothermal chromatography is an ideal method to rapidly and continuously separate short-lived volatile radionuclides from less volatile species [12].

To extract the $-\triangle H_{ads}$ of the species on different surfaces, a Monte Carlo Simulation (MCS) based on an existing code for circular detector channels developed by Zvara is often used [11, 48]. The original code was adapted for a rectangular detector channel [49] and successfully used for the analysis of several experimental data given in refs. [10, 25, 33, 43].

In this simulation, the path of the atom or molecule through the detector column is simulated. Starting the simulation, based on the half-life of the isotopes, a random lifetime is determined. The atom spends its lifetime either adsorbed on the surface or in the carrier gas in transport along the column. After every ad- and desorption step, the lifetime is compared to the sum time of all adsorption and flight steps. If this sum exceeds the lifetime of the isotope, the position at which it decays is recored and the next atom is simulated. By repetition of such simulations for one single atom 10^7 times, the distribution pattern of nuclei decayed in the column is obtained for a given $-\triangle H_{ads}$.

The MCS does not only take into account the geometry of the detector column, but also information of the carrier gas, e.g., pressure and flow rates inside the RTC, as well as the temperature along the detector column. In this way, it is possible to simulate distribution patterns of the isotope under experimental conditions. To determine the limit for $-\triangle H_{ads}$ in the case of diffusion controlled deposition, the experimental rate per detector, decreasing along the chromatography channel and approaching a plateau is fitted with a linear regression, and a 95% prediction band is determined. This prediction band is the area in which 95% of all our experimental data points are covered. We simulate the distribution pattern in the detector channel with the MCS approach for different values of the adsorption enthalpy and compare these patterns to the 95% prediction band. The lowest adsorption enthalpy value corresponding to the distribution pattern lying fully inside the prediction band is the lower limit of the adsorption enthalpy for the diffusion controlled deposition.

Figs. 3a,b show the experimental distribution patterns of $^{182-183}$Hg on a Au-covered COMPACT detector array, produced in the ^{50}Ti+^{140}Ce reaction.

In Fig. 3a, the Hg isotopes were thermalized and flushed out of the RTC into the COMPACT detector array by Ar gas, whereas in Fig. 3b, a gas mixture of 70% He and 30% Ar was used. The gas pressures and gas flow rates can be taken from the caption of the figure. The addition of He gas narrows the distribution pattern of Hg on the Au-covered COMPACT detector array. The presence of He gas causes the Hg atoms to diffuse faster towards the wall of the
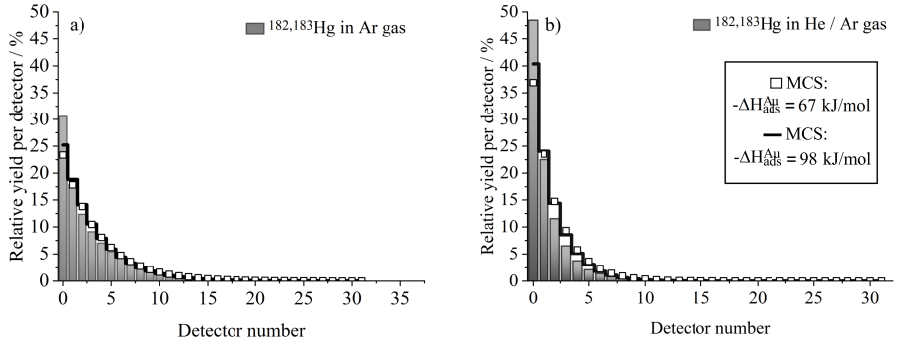
Fig. 3: Distribution patterns of $^{182-183}$Hg on a Au-covered COMPACT detector. Panel a, shows the distribution in pure Ar gas obtained in the energy range 5.0 - 6.4 MeV, with a gas pressure inside the RTC of about 0.9 bar, and a gas flow rate of 1.7 L/min. Panel b shows the distribution (3.0 - 6.0 MeV) in a gas mixture of 70% He, and 30% Ar, with a similar gas pressure, but a gas flow rate of 1.5 L/min. Furthermore MCS with different -$\triangle H_{ads}$ are shown for both distributions. The MCS were performed with the same gas pressure and gas flow rates as used in the experiments.

detector, where they will be immobilized and undergo decay. Whereas in Ar gas, Hg can be transported further along the detector column, before colliding to the walls and undergoing decay. This deposition process inside the detector column, which occurs for strongly interacting species, is termed as diffusion-controlled deposition. This does not allow to obtain detailed information on the strength of the surface interaction for -$\triangle H_{ads}$ values that are higher than the -$\triangle H_{ads}$ limit for diffusion-controlled deposition, but depends largely on the composition and dynamics of the gas.

Based on the above mentioned method, many Monte-Carlo simulations using different values for the -$\triangle H_{ads}$ were performed to determine the -$\triangle H_{ads}$ limit for Hg on Au. All those simulations using -$\triangle H_{ads} \geq$ 67 kJ/mol resulted in distributions that were fully contained inside the 95% prediction band, hence, our result is $-\Delta H_{ads}^{Au}$(Hg) $\geq$ 67 kJ/mol (95% c.i.). Fig. 3 shows the simulated distribution pattern in both gases for $-\Delta H_{ads}^{Au}$(Hg)=67, and 98 kJ/mol. Both MCS are in fairly good agreement with the experimental determined distribution pattern. The simulations of $-\Delta H_{ads}^{Au}$(Hg)=67 and 98 kJ/mol exhibit similar relative yield values per detector, as a consequence that $-\Delta H_{ads}^{Au}$(Hg)=98 kJ/mol is above the diffusion controlled deposition limit.

2.3 Influence of background on the measurements

In Fig. 4, the sum spectrum of the background measured in COMPACT I and COMPACT II is shown. The energy spectrum was permanently monitored with a minor ^{219}Rn activity, added to the carrier gas. In addition a small contamination on the third PIN diode of COMPACT I, with the non-volatile isotopes ^{223}Ra and ^{211}Bi was detected. This caused a high background in the third and following PIN diodes of COMPACT I. Due to this, a background subtraction was applied to the spectra collected during irradiation periods in all detector pairs. This was of particular importance for the measurement of ^{185,186}Pb, due to the overlap of their α-decay energies with those of ^{211}Bi.
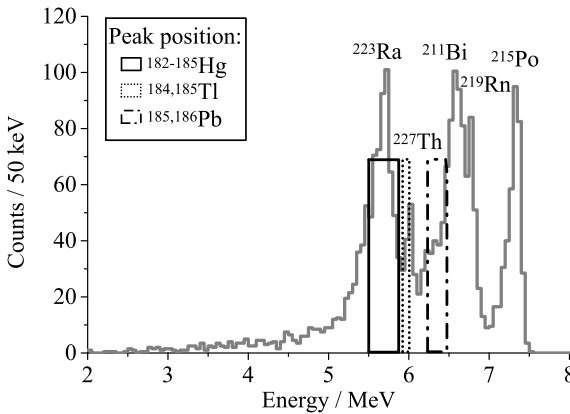

Fig. 4: Background α-energy spectrum of a ^{227}Ac contamination in the COMPACT I- and II detector array. The peak position of Hg, Tl, and Pb isotopes are included. The measurement was done in 27 minutes of irradiation time in Ar carrier gas at a flow rate of 2.2 L/min.

3 Results and Discussion

The experimental distribution pattern of Hg, Tl, and Pb were evaluated from measured α-sum spectra obtained by each Pin diode pair of COMPACT I (SiO$_2$-covered) and COMPACT II (Au-covered) detector arrays.

As shown in section 2.2, we can only determine $-\Delta H_{ads}$ limits due to the diffusion controlled deposition. This is why the following observed adsorption properties of Hg, Tl, and Pb are compared and evaluted to $-\Delta H_{ads}$ values obtained in former experiments, shown in Tab. 3.

Table 3: Adsorption enthalpies ($-\Delta H_{ads}$ in kJ/mol) of Hg, Tl, TlOH, and Pb on SiO₂ and Au surfaces, determined in former experiments.

	Pb	Tl	TlOH	Hg
$-\Delta H_{ads}^{Au}$	234 [31]	270±10 [29]	146±3 [29]	98±3 [28]
$-\Delta H_{ads}^{SiO_2}$	165±4 [28]	112±5 [29]	134±5 [29]	42±2 [28]

3.1 Adsorption of Hg on SiO₂ and Au surfaces

In Fig. 5a the experimental sum spectrum of Hg isotopes, produced using a ⁵⁰Ti beam on a ¹⁴⁰Ce target measured with COMPACT I (SiO₂-covered) and COMPACT II (Au-covered), is shown. According to the HIVAP calculations the most intense decay channels are the 8, 7, 6n, corresponding to $^{182-184}$Hg.

A broad single peak at 5.8 to 5.9 MeV is visible in the spectrum, originating from ^{182,183}Hg, see Tab. 1. No clear peak from ^{184}Hg can be observed, due to its small yield (<3% of ^{184}Hg) in ⁵⁰Ti-induced reactions and the energy resolution in the COMPACT detectors in Ar gas. Furthermore, due to the FWHM of ≈200 keV and a long tail at the low energy side of the peak, the α lines of $^{182-184}$Hg are not resolved. Nevertheless, a small contribution of ^{184}Hg cannot be excluded in the distribution over the entire energy area.

In Fig. 5b the distribution pattern of $^{182-184}$Hg along the COMPACT I and II detector arrays is shown. To obtain the distribution pattern, the number of counts in the energy range of 5.0 to 6.4 MeV was integrated for each individual PIN diode pair. The distribution pattern reflects the deposition of the atoms in the detector array, which is related to the adsorption strenght, half-life of the isotopes, and the ratio between the temperature- and pressure- dependent diffusion speeds of the species and carrier gas velocities.

A small fraction of only 1% of $^{182-184}$Hg was detected in COMPACT I, equally distributed along the 32 PIN diodes. The low detection rate and uniform distribution along the detector array suggests that these events are caused by
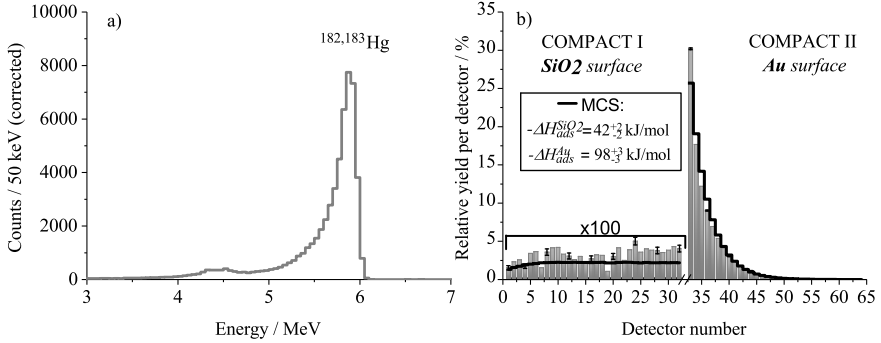
Fig. 5: Sum spectrum of $^{182-184}$Hg in COMPACT I+II measured in pure Ar gas (panel a). Comparison of the measured $^{182-184}$Hg distribution (grey bars) on SiO$_2$ (COMPACT I) and Au (COMPACT II) surfaces. To obtain the distribution pattern, the number of counts in the energy range of 5.0 to 6.4 MeV was integrated for each individual PIN diode pair. Statistical fluctuations are indicated by the error bars on every 4th COMPACT detector. The experimental data of COMPACT I are multiplied by factor 100, to visualise them in the graphics. Black lines show results of MCS using -$\triangle H_{ads}$ values from Ref.[31, 28] (panel b).

Hg decaying in-flight migrating along the SiO$_2$-covered COMPACT I array. The adsorption enthalpy value for Hg on SiO$_2$ was determined as $-\Delta H_{ads}^{SiO_2}$(Hg)=43±1 kJ/mol (95% c.i.) and is in agreement with the data $-\Delta H_{ads}^{SiO_2}$(Hg)=42±2 kJ/mol taken from Lit. [28]. The simulated distribution for the literature value is also shown in Fig. 5b.

In contrast, a much higher and exponentially decreasing rate along the COMPACT II detector array was observed. The observed distribution of $^{182-184}$Hg in COMPACT II on the Au surface points to the formation of metallic bonds with Au. The distribution of Hg on Au obtained via a MCS using $-\Delta H_{ads}^{Au}$(Hg)=98±3 kJ/mol [31] describes our experimental observation well and is in line with our determined limit for $-\Delta H_{ads}^{Au}$(Hg) of ≥67 kJ/mol (95% c.i.).

3.2 Adsorption of Pb on SiO$_2$ and Au surfaces

A variety of Pb isotopes were produced in the reaction ^{142}Nd(^{50}Ti,xn)$^{192-x}$Pb. For this fusion-evaporation reaction, HIVAP calculations predict the highest production rates for $^{185-187}$Pb, see Tab. 1.

Due to the smaller production rates of $^{185-187}$Pb compared to Hg, the experiment was performed at a high beam intensity, i.e., with a high beam pulse

repetition rate of 45 Hz of the pulsed ^{50}Ti^{8+} beam. Like this, the rate of Pb events could be increased with respect to those produced by the ^{211}Bi.

In Fig. 6, the spectra measured in COMPACT I (SiO$_2$-covered) and COMPACT II (Au-covered) are shown. In the COMPACT I spectrum, a peak at 6.3 to 6.4 MeV can be seen, which can clearly be attributed to ^{185,186}Pb. This peak does not appear in the COMPACT II spectrum. No clear peak of ^{187}Pb is visible, because of its small yield in ^{50}Ti induced reactions.
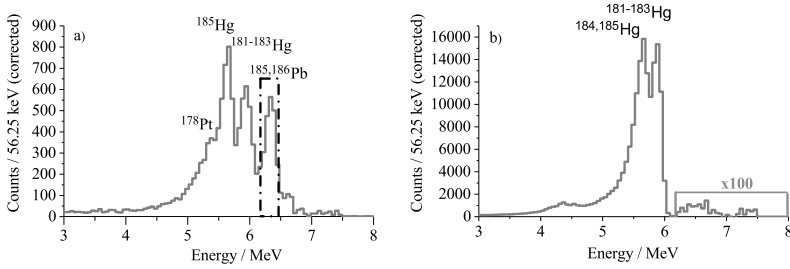

Fig. 6: Sum spectra of Pb and Hg isotopes in COMPACT I (panel a) and COMPACT II (panel b), measured in Ar gas.

In Fig. 7a, the distribution pattern of ^{185,186}Pb is shown, which is exponentially decreasing along the COMPACT I detector array. Furthermore the results of MCS with $-\Delta H_{ads}^{SiO_2}$(Pb)=165±4 kJ/mol, given in ref. [28], are shown. They agree with expectations based on the known strong interaction between Pb atoms and the SiO$_2$ surface. For Hg as well as for Pb, the exponentially decreasing distribution is due to a diffusion-controlled deposition process. Adopting also for the deposition of Pb on SiO$_2$, the lower limit for the adsorption enthalpy of 67 kJ/mol (95% c.i.), which was determined for Hg on Au, leads to a modeled distribution, which describes the experimental data well, see Fig. 7a.

At lower α-particle energies, two additional peaks are visible in Fig. 6a. The peak at about 5.6 MeV can be attributed to ^{185}Hg, whereas the peak at 5.8 to 5.9 MeV can be assigned to $^{181-183}$Hg. In the sum spectrum of the Au-covered COMPACT detector, see Fig. 6b, two prominent peaks can be observed, which can all be attributed to isotopes of Hg. At an energy of 5.5 to 5.6 MeV a peak from the decay of ^{184,185}Hg can be seen. The peak at the highest energy originates from $^{181-183}$Hg. As summarized in Tab. 1, the reaction ^{50}Ti+^{142}Nd allows the production of Hg isotopes in different reaction paths, i.e., either as daughters of Pb isotopes after one α-decay or after two consecutive EC/β^+-decays. Furthermore,

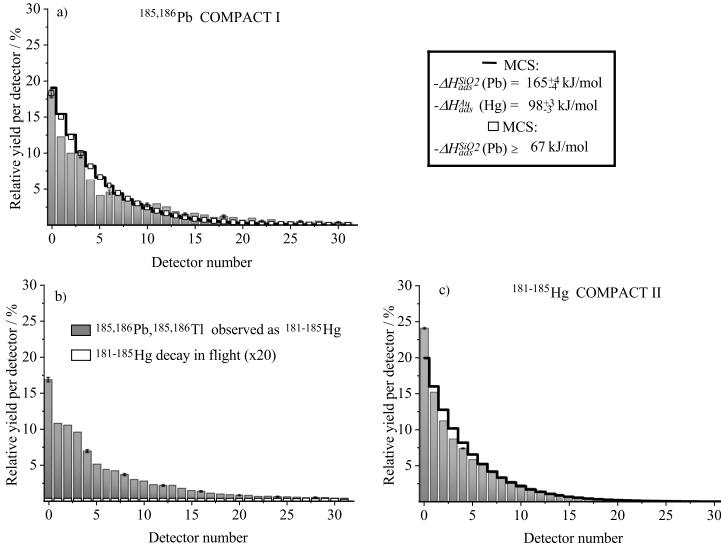**Fig. 7:** Distributions along the COMPACT detector arrays and statistical fluctuations indicated by error bars on every 4th detector are illustrated. Panel a shows the measured Pb distribution (6.2-6.5 MeV) and the results of the MCS using the $-\triangle H_{ads}$ value from Ref. [28], as also the adsorption enthalpy limit of 67 kJ/mol in COMPACT I (SiO$_2$-covered). Panel b (5.4-6.1 MeV) and c (3.0-6.5 MeV), show the Hg distributions along COMPACT I and COMPACT II (Au-covered), respectively.

Hg isotopes can be produced abundantly in evaporation channels: either directly in αxn channels, or indirectly in $p x$n channels as EC/β^+-decay products of Tl isotopes.

The adsorption behavior of directly produced Hg isotopes on SiO$_2$ and Au surfaces was already discussed in section 3.1. Hg interacts only weakly with SiO$_2$ surfaces, and can be transported to the Au-covered COMPACT II detector with a high efficiency, as shown in Fig. 7c. Hg isotopes, produced after the decay of Pb and Tl isotopes, can be immobilized on the SiO$_2$ surface, and thus exhibit a similar exponential distribution as Pb or Tl. If Hg atoms, following β^+- or α decay, recoil into the open gas channel, they can be transported further to the Au-covered COMPACT II detector, and will adsorb there. The rate of Hg in COMPACT II is much higher than in COMPACT I (cf. Fig. 6). This indicates that the majority of Hg adsorbed in COMPACT II (cf. Fig. 7b) was probably

produced directly in the αxn channel, or after α, or β^+/EC decays of Tl and Pb inside the RTC. The Hg distribution along COMPACT I (see Fig. 7b), shows a combination of both reaction paths. The exponential distribution along the first detectors of COMPACT I looks similar to the distribution of Pb (see Fig. 7a) pointing to the fact that most of Hg isotopes detected on the SiO$_2$ surface originate from Hg immobilized after the decay of Pb or Tl. The Hg yield does not approach zero even in the last detectors of COMPACT I. This is due to decay in flight mainly of directly produced Hg isotopes, which are transported to COMPACT II and adsorb there.

3.3 Adsorption of Tl on SiO$_2$ and Au surfaces

In Figs. 8a and 8b the Tl spectra measured in COMPACT I and II are shown. Short-lived Tl isotopes were produced in the reaction ^{141}Pr(^{50}Ti, xn)$^{191-x}$Tl. According to the HIVAP calculations, see Tab. 1, $^{183-185}$Tl are produced and detected. Of note are their small α-decay branches, see Tab. 1, which render the detection of these isotopes via α-decay challenging.

The spectra in COMPACT I and II show two main broad α-peaks. The first peak around 5.5 MeV, can be attributed to the decay of ^{184,185}Hg and the second at 5.9 MeV to ^{183}Hg.

In the ^{50}Ti+^{141}Pr reaction, Hg isotopes can be produced in two different reaction paths, see Tab. 1. They can either be produced as daughters of Tl isotopes after EC/β^+-decay, or directly in $p x$n reactions. The produced Hg isotopes have much larger α branches than the Tl isotopes, see Tab. 1.

The larger rate of Hg decays in COMPACT II in comparison with COMPACT I, points to a high production of Hg in the direct $p x$n reaction, as well as Hg produced via decay of Tl inside the RTC. Although the detected α-decay lines in COMPACT I can clearly be attributed to isotopes of Hg, the observed exponentially decreasing distribution pattern in COMPACT I up to detector number 15 (cf. Fig. 8c) points to a much stronger interaction with the SiO$_2$ surface than was determined for directly produced Hg (cf. sect. 3.1). This observation can only be explained with immobilized volatile Hg atoms on the SiO$_2$ surface after the β^+ decay of Tl. Decay in flight of Hg is clearly visible beyond detector number 15, and Hg is transported towards the COMPACT II detector.

The observed distribution pattern in the COMPACT I array suggests that Tl adsorbs strongly on a SiO$_2$ surface. This is in agreement with results from the literature,where values of $-\Delta H_{ads}^{SiO_2}$(Tl)=112±5 kJ/mol [30] and 158±3 kJ/mol [32] and $-\Delta H_{ads}^{SiO_2}$(TlOH)=134±5 kJ/mol [29] were obtained. The authors of Ref. [29] observed that Tl atoms are very sensitive to O$_2$ and H$_2$O impurities in the gas
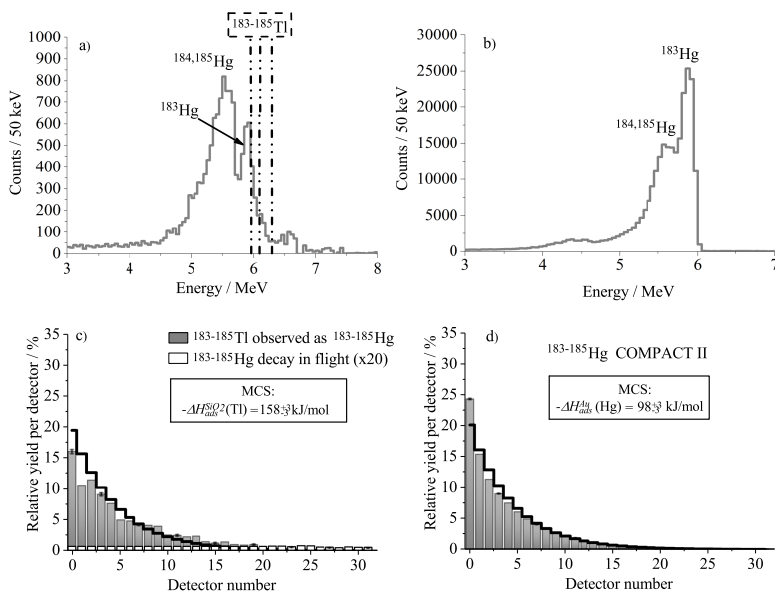
Fig. 8: Panels a)and b) show the sum spectra of Hg in COMPACT I and II. In panels c) and d) the distribution (with statistical uncertainties indicated as error bars in every fourth experimental bar) of Hg (3.5-6.5 MeV) inside the COMPACT detector arrays, together with the result of the MCS using the $-\Delta H_{ads}$ for Tl from Ref [32] is shown. The white bars shown in panel c, shows Hg decay in flight, determined from the total sum of Hg, subtracted the deposition of Tl.

and on surfaces. The presence of these impurities led to reactions forming TlOH. Using SiO_2 as a solid phase for the interaction with Tl atoms adsorbing from the gas phase, the formation of TlOH on the surface was inferred [29]. Presumably, this was similar in the earlier work reported in [30]. Theoretical studies agree that reactions of Tl with the SiO_2 surface are likely [20]. Our experimental results do not give a clear indication which chemical species of Tl was observed in our experiments. Based on the above discussion, MCS were performed assuming TlOH was formed on the SiO_2 surface (cf. Fig. 8c). Comparing these simulations with experimental results, we observed a good agreement in the COMPACT I, while the distribution pattern of Hg in COMPACT II (cf. Fig. 8d) shows the typical chemical behavior of diffusion controlled deposition of Hg on Au.

3.4 Chemical yield

The overall chemical yield for transporting Hg and Pb from the RTC to the COMPACT setup was measured in a subsequent experiment. Short-lived Hg and Pb isotopes were produced in the reactions ^{142}Nd(^{48}Ca,6-8n)$^{182-184}$Hg, and ^{144}Sm(^{48}Ca,5-7n)$^{185-187}$Pb, see Tab. 2. They were thermalized in the RTC (window size:(40x60) mm^2, depth (20 mm) and transported with a PTFE capillary of 5-cm length ($\oslash$ 3 mm) to a series of two COMPACT detector arrays (COMPACT I, SiO$_2$- and COMPACT II, Au-covered), at a gas flow rate of 2 L/min (30% He/ 70% Ar). Both detectors were operated at room temperature (21°C). The RTC was separated from TASCA by a 6 μm thick Mylar window, which was supported by a stainless steel grid with 80% geometrical transmission. The rate at which Hg and Pb atoms entered the RTC was determined in separate experiments, where they implanted into a (48x72) mm^2 double-sided silicon strip detector with 16 strips each in x-and y-direction, referred to as the Focal Plane Detector (FPD). The FPD was installed directly behind the RTC window. The calculated geometrical efficiency for detecting an α-particle emitted by a Hg or Pb isotope implanted in the FPD is 55%. Due to the interference of signals from implanted recoils with the ones from α particles, only the data collected during the beam off periods were evaluated. Identically, also for measurements with COMPACT, only data collected during beam-off periods were used. The rate of events originating from the decay of Hg and Pb isotopes, both in the FPD as also in the COMPACT detector arrays, was integrated in the energy range of 4.8-6.12 MeV for Hg and 5.5-6.5 MeV for Pb. In Tab. 4, the count rates as well as the projectile doses for the experiments are listed.

The chemical yield, was determined to 62±0.5% for Hg and 25±1% for Pb. The lower yield for Pb is, due to adsorption losses of the less volatile Pb on the walls of the RTC and the tube connecting the RTC to COMPACT.

Table 4: Important parameters for the chemical yield determination of short-lived isotopes of Hg and Pb. The uncertainty for the projectile dose was calculated with about 10% [34]. The total amount of counts were determined in the energy ranges 4.8-6.12 MeV for Hg and 5.5-6.5 MeV for Pb.

	Hg	Pb
Energy range [MeV]	**4.8-6.12**	**5.5-6.5**
FPD		
Projectile dose	$2.6 \cdot 10^{14}$ *(0.3)*	$7.1 \cdot 10^{14}$ *(0.7)*
Counts	48744 *(221)*	22937 *(151)*
COMPACT	**Au surface**	**SiO$_2$ surface**
Projectile dose	$2.5 \cdot 10^{14}$ *(0.3)*	$5.7 \cdot 10^{14}$ *(0.6)*
Counts	41403 *(203)*	6768 *(82)*

4 Conclusion

Online chemical adsorption studies with single short-lived atoms of Hg, Tl, and Pb have been performed. The radioisotopes with half-lives in the range of 4-49 s were produced in fusion-evaporation reactions and isolated in the gas-filled recoil separator TASCA. Two COMPACT detector arrays, where the first contained SiO_2 - and the second one Au-covered surfaces, kept at room temperature, were used to study the interaction of the three elements in this setup. The PTFE was the sole surface material encountered by the studied elements prior to reaching the COMPACT detectors.

Tl and Pb adsorbed on the SiO_2 surface. The decay of only a small amount of Hg, uniformly distributed along the SiO_2-covered COMPACT array, was observed, and is interpreted to originate from decay in flight. This points to a weak interaction of Hg with a SiO_2 surface. The majority of the Hg reached the Au-covered COMPACT array, where it readily adsorbed. The observed distribution patterns of Hg, Tl, and Pb agree with former experimental observations, confirming our used setup to be suitable for performing on-line chemical studies with single short-lived radioisotopes. A lower limit for the $-\Delta H_{ads}$ of Tl and Pb on SiO_2 as well as for Hg on Au of 67 kJ/mol (95% c.i.) was determined. The adsorption enthalpy value for Hg on SiO_2 of 43±1 kJ/mol (95% c.i.) was obtained. Both adsorption enthalpies are in agreement with former work [23, 28, 29, 30, 31, 32].

With this experimental setup, it is possible to chemically separate Hg, Tl, and Pb and compare their interaction strength with the surface coverage material, thus enabling comparative studies of the interaction of these elements along with their heavier homologs, the transactinides Cn, Nh, and Fl.

References

[1] Schädel, M.: Chemistry of Superheavy Elements. Angew. Chem. Int. Ed. **45**, 368 (2006)

[2] Öhrström, L., Reedijk, J.: Names and symbols of the elements with atomic

numbers 113, 115, 117 and 118. (IUPAC Recommendations 2016), Pure Appl. Chem. **88** (12), 1225-1229 (2016)

[3] Pyykkö, P.: Relativistic effects in structural chemistry. Chem. Rev. **88**, 563-594 (1988)

[4] Fricke, B.: Superheavy Elements: A Prediction of their Chemical and Physical Properties. Springer Verlag, Berlin Heidelberg GmbH **21**, 89-144 (1975)

[5] Pyykkö, P., Desclaux, J. P.: Relativity and the Periodic System of Elements. Acc. Chem. Res. **12**(8), 276-281 (1979)

[6] Schädel, M., Shaughnessy, D.: The Chemistry of Superheavy Elements. Second Edition, Springer-Verlag Berlin/ Heidelberg (2014)

[7] Düllmann, Ch. E.: Physical separators for the heaviest elements. Nucl. Instrum. Meth. Phys. Research B **266**, 4123-4130 (2008)

[8] Schädel, M.: Superheavy element chemistry at GSI-status and perspectives. Eur. Phys. J. D **45**, 67-74 (2007)

[9] Schädel M., Ackermann D., Andersson L.-L., Ballof J., Block M., Buda R. A., Brüchle W., Dragojevic I., Düllmann Ch. E., Dvorak J., Eberhardt K., Even J., Gates J. M., Gerl J., Gorshkov A., Golubev P., Graeger R., Gregorich K. E., Gromm E., Hartmann W., Heßberger F. P., Hild D., Hoischen R., Hübner A., Jäger E., Khuyagbaatar J., Kindler B., Kojouharov I., Kratz J. V., Krier J., Kurz N., Lahiri S., Liebe D., Lommel B., Maiti M., Mendel M., Merchan E., Nitsche H., Nayak D., Nilssen J., Omtvedt J. P., Opel K., Reichert P., Rudolph D., Sabelnikov A., Samadani F., Schaffner H., Schausten B., Schuber R., Schimpf E., Semchenkov A., Stavsetra L., Steiner J., Szerypo J., Thörle-Pospiech P., Toyoshima A., Türler A., Uusitalo J., Wiehl N., Wollersheim H.-J., Wunderlich T., Yakushev A.: TASCA Commissioning Completed. GSI Scientific Report, 138-139 (2008)

[10] Türler, A., Eichler, R., Yakushev, A.: Chemical studies of elements with Z≥ 104 in gas phase. Nucl. Phys. A **944**, 640-689 (2015)

[11] Zvara, I.: The Inorganic Radiochemistry of Heavy Elements. Springer Science, (2008)

[12] Türler, A., Pershina, V.: Advances in the Production and Chemistry of the Heaviest Elements. Chem. Rev. **113** (2), 1237-1312 (2013)

[13] Eichler, B.: Das Flüchtigkeitsverhalten von Transactiniden im Bereich um Z=114 (Vorraussage). Kernenergie **19**, 307-311 (1976)

[14] Pershina, V., Bastug, T., Jacob, T., Fricke, B., Varga, S.: Intermetallic compounds of the heaviest elements: the electronic structure and bonding of dimers of element 112 and its homolog Hg. Chem. Phys. Lett. **365**, 176-183 (2002)

[15] Pershina, V., Anton, J., Jacob, T.: Theoretical predictions of adsorption

behavior of elements 112 and 114 and their homologs Hg and Pb. J. Chem. Phys. **131**, 084713 (2009)

[16] Eichler, R., Aksenov, N. V., Albin, Yu. V., Belozerov, A. V., Bozhikov, G. A., Chepigin, V. I., Dmitriev, S. N., Dressler, R., Gäggeler, H. W., Goshkov, V. A., Henderson, R. A., Johnsen A. M., Kenneally, J. M., Lebedev, V. Ya., Malyshev, O. N., Moody, K. J., Oganessian, Yu. Ts., Petrushkin, O. V., Piguet, D., Popeko, A. G., Rasmussen, P., Serov, A., Shaughnesy, D. A., Shishin, S. V., Shutov, A. V., Stoyer, M. A., Stoyer N. J., Svirikhin, A. I., Tereshatov, E. E., Vostokin, G. K., Wegrzecki, M., Wilk, P. A., Wittwer, D., Yeremin, A. V.: Indication for a volatile element 114. Radiochim. Acta **98**, 113-139 (2010)

[17] Pershina, V.: A relativistic periodic DFT study on interaction of superheavy elements 112 (Cn) and 114 (Fl) and their homologs Hg and Pb, respectively, with a quartz surface. Phys. Chem. Chem. Phys. **18**, 17750-17756 (2016)

[18] Schwerdtfeger, P., Seith, M.: Relativistic Effects of the Superheavy Elements. Encyclopedia of Computational Chemistry. Wiley New-York **4**, 2480-2409 (1998)

[19] Desclaux, J. P.: Relativistic Dirac-Fock expectation values for atoms with Z=1 to Z=120, Atomic Data and Nuclear Data Tables. **V 12 Issue 4**, 311-406 (1973)

[20] Pershina, V.: A Theoretical Study on the Adsorption Behavior of Element 113 and Its Homologue Tl on a Quartz Surface: Relativistic Periodic DFT Calculations. J. Phys. Chem. C **120** (36), 20232-20238 (2016)

[21] Pershina, V.: Electronic structure and properties of superheavy elements. Nucl. Phys. A **944**, 578-613 (2015)

[22] Pershina, V., Anton, J., Jacob, T.: Electronic structures and properties of MAu and MOH, where M=Tl and element 113. Chem. Phys. Lett. **480**, 157-160 (2009)

[23] Eichler, R., Aksenov, N. V., Belozerov, A. V., Boshikov, G. A., Chepigin, V. I., Dmitriev, S. N., Dressler, R., Gäggeler, H. W., Gorshkov, V. A., Haenssler, F., Itkis, M. G., Laube, A., Lebedev, V. Ya., Malyshev, O. N., Oganessian Yu. Ts., Petrushkin, O. V., Piguet, D., Rasmussen, P., Shishkin S. V., Shutov, A. V., Svirikhin, A. I., Tereshatov, E. E., Vostokin, G. K., Wegrzecki, M., Yeremin A. V.: Chemical characterization of element 112. Nature **447**, 72-75 (2007)

[24] Eichler, R., Aksenov, N. V., Belozerov, A. V., Boshikov, G. A., Chepigin, V. I., Dmitriev, S. N., Dressler, R., Gäggeler, H. W., Gorshkov, V. A., Haenssler, F., Itkis, M. G., Laube, A., Lebedev, V. Ya., Malyshev, O. N., Oganessian Yu. Ts., Petrushkin, O. V., Piguet, D., Popeko, A. G., Rasmussen, P., Shishkin S. V., Serov, A. A., Shutov, A. V., Svirikhin, A. I., Tereshatov, E. E., Vostokin,

G. K., Wegrzecki, M., Yeremin A. V.: Thermodynamische und physikalische Eigenschaften von Element 112. Angew. Chem. **120(17)**, 3306-3310(2008)

[25] Yakushev, A., Gates, J. M., Türler, A., Schädel, M., Düllmann, Ch. E., Ackermann, D., Andersson, L. L., Block, M., Brüchle, W., Dvorak, J., Eberhardt, K., Essel, H. G., Even, J., Forsberg, U., Gorshkov, A., Graeger, R., Gregorich, K. E., Hartmann, W., Herzberg, R. D., Heßberger, F. P., Hild, D., Hübner, A., Jäger, E., Khuyagbaatar J., Kindler, B., Kratz, J. V., Krier, J., Kurz, N., Lommel, B., Niewisch, L. J., Nitsche, H., Omtvedt J. P., Parr, E., Qin, Z., Rudolph, D., Runke, J., Schausten, B., Schimpf, E., Semchenkov, A., Steiner, J., Thörle-Pospiech, P., Uusitalo, J., Wegrzecki, M., Wiehl, N.: Superheavy Element Flerovium (Element 114) is a Volatile Metal. Inorg. Chem. **53**, 1624-1629 (2014)

[26] Dmitriev, S. N., Aksenov, N. V., Albin, Y. V., Bozhikov, G. A., Chelnokov, M. L., Chepigin, V. I., Eichler, R., Isaev, A. V., Katrasev, D. E., Lebedev V. Ya., Malyshev, O. N., Petrushkin, O. V., Porobanuk, L. S., Ryabinin, M. A., Sabel´nikov, A. V., Sokol, E. A., Svirikhin, A. V., Starodub, G. Ya., Usoltsev, I., Vostokin, G. K., Yeremin, A. V.: Pioneering experiments on the chemical properties of element 113. Mendeleev Commun. **24**, 253-256 (2014)

[27] Aksenov, N. V., Steinegger, P., Abdullin, F. Sh., Albin, Y. V., Bozhikov, G. A., Chepigin, V. I., Eichler, R., Lebedev V. Ya., Madumarov, A. Sh., Malyshev, O. N., Petrushkin, O. V., Polyakov, A. N., Popov, Y. A., Sabel´nikov, A. V., Sagaidak, R. N., Shirokovsky, I. V., Shumeiko, M. V., Starodub, G. Ya., Tsyganov, Y. S., Utyonkov, V. K., Voinov, A. A., Vostokin, G. K., Yeremin, A. V., Dmitriev, S. N.: On the volatility of nihonium (Nh, Z = 113). Eur. Phys. J. A **53**, 158 (2017)

[28] Soverna, S.: Attempt to chemically characterize element 112. Inauguraldissertation der Philosophisch-naturwissenschaftlichen Fakultät der Universität Bern (2004)

[29] Serov, A., Eichler, R., Dressler, R., Piguet, D., Türler, A., Vögele, A., Wittwer, D., Gäggeler, H. W.: Adsorption interaction of carrier-free thallium species with gold and quartz surfaces. Radiochim. Acta **101**, 421-425 (2013

[30] Eichler, B.: Das Verhalten flüchtiger Radionuklide im Temperaturgradientenrohr unter Vakuum. Report **ZFK-346**, Zentralinstitut Kernforschung Dresden (1977)

[31] Soverna, S., Dressler, R., Düllmann, Ch. E., Eichler, B., Eichler, R., Gäggeler, H. W., Haenssler, F., Niklaus, J. -P., Piguet, D., Qin, Z., Türler, A., Yakushev, A. B.: Thermochromatographic studies of mercury and radon on transition metal surfaces. Radiochim. Acta. **93**, 1-8 (2005)

[32] Steinegger, P., Asai, M., Dressler, R., Eichler, R., Kaneya, Y., Mitsukai, A., Nagame, Y., Piguet, D., Sato, T. K., Schädel, M., Takeda, S., Toyoshima, A.,

Tsukada, K., Türler, A., Vascon, A.: Vacuum Chromatography of Tl on SiO_2 at the Single-Atom Level. J. Phys. Chem. C **120** (13), 7122-7132 (2016)

[33] Yakushev, A.: Chemical Characterization of Element 108, Hassium and Snythesis of New Hassium Isotopes. Habilitation Thesis in the Field of Radiochemistry at Technical University of Munich (2009)

[34] Gates, J. M., Düllmann, Ch. E., Schädel, M., Yakushev, A., Türler, A., Eberhardt, K., Kratz, J. V., Ackermann, D., Andersson, L.-L., Block, M., Brüchle, W., Dvorak, J., Essel, H. G., Ellison, P. A., Even, J., Forsberg, U., Gellanki, J., Gorshkov, A., Graeger, R., Gregorich, K. E., Hartmann, W., Herzberg, R. -D., Heßberger, F. P., Hild, D., Hübner, A., Jäger, E., Khuyagbaatar, J., Kindler, B., Krier, J., Kurz, N., Lahiri, S., Liebe, D., Lommel, B., Maiti, M., Nitsche, H., Omtvedt, J. P., Parr, E., Rudolph, D., Runke, J., Schaffner, H., Schausten, B., Schimpf, E., Semchenkov, A., Steiner, J., Thörle-Pospiech, P., Uusitalo, J., Wegrzecki, M., Wiehl, N.: First superheavy element experiments at the GSI recoil separator TASCA: The production and decay of element 114 in the $^{244}Pu(^{48}Ca,3\text{-}4n)$ reaction. Phys. Rev. C **83**, 054618-1-17 (2011)

[35] Jäger, E., Brand, H., Düllmann, Ch. E., Khuyagbaatar, J., Krier, J., Schädel, M., Torres, T., Yakushev, A.: High Intensity target wheel at TASCA : target wheel control system and target monitoring. J. Radioanal Nucl. Chem. **299**, 1073-1079 (2014)

[36] Semchenkov, A., Brüchle, W., Jäger, E., Schimpf, E., Schädel, M., Mühle, C., Klos, F., Türler, A., Yakushev, A., Belov, A., Belyakova, T., Kaparkova, M., Kukhtin, V., Lamzin, E., Sytchevsky S.: The TransActinide Separator and Chemistry Apparatus (TASCA) at GSI-Optimization of ion-optical structures and magnet designs. Nucl. Instr. and Meth. in Phys. Res. B **266**, 4153-4161 (2008)

[37] Reisdorf, W., Schädel, M.: How well do we understand the synthesis of heavy elements by heavy-ion induced fusion?. Z. Phys. A **343**, 47-57 (1992)

[38] Chu, S. Y. F., Ekström, L. P., Firestone, R. B.: The Lund / LBNL Nuclear Data Search. **Version 2.0** (1999)

[39] IAEA Nuclear Data Section, Nuclear Data Sheets **111**, 275 (2010)

[40] Even, J., Ballof, J., Brüchle, W., Buda, R. A., Düllmann, Ch. E., Eberhardt, K., Gorshkov, A., Gromm, E., Hild, D., Jäger, E., Khuyagbaatar, J., Kratz, J. V., Krier, J., Liebe, D., Mendel, M., Nayak, D., Opel, K., Omtvedt, J. P., Reichert, P., Runke, J., Sabelnikov, A., Samadani, F., Schädel, M., Schausten, B., Scheid, N., Schimpf, E., Semchenkov, A., Thörle-Pospiech, P., Toyoshima, A., Türler, A., Vicente Vilas, V., Wiehl, N., Wunderlich, T., Yakushev, A.: The recoil transfer chamber- An interface to connect the physical preseparator

TASCA with chemsitry and counting setups. Nucl. Instrum. Methods Phys. Res. Sect. A **638**, 157-164 (2011)

[41] Ziegler, J. F., Ziegler, M. D., Biersack, J. P.: SRIM- The stopping and range of ions in matter (2010). Nucl. Instrum. Methods Phys. Res. Sect. B: Beam Interactions with Materials and Atoms **268**, 1818-1823 (2010)

[42] Ziegler J. F.: SRIM - The Stopping Range of Ions in Matter, www.srim.org, Downloaded: 08.10.2014, (2013)

[43] Even, J., Yakushev, A., Düllmann, Ch. E., Haba, H., Asai, M., Sato, T. K., Brand, H., Di Nitto, A., Eichler, R., Fan., F. L., Hartmann, W., Huang, M., Jäger, E., Kaji, D., Kanaya, J., Kaneya, Y., Khuyagbaatar, J., Kindler, B., Kratz, J. V., Krier, J., Kudou, Y., Kurz, N., Lommel, B., Miyashita, S., Morimoto, K., Morita, K., Murakami, M., Nagame, Y., Nitschen, H., Ooe, K., Qin, Z., Schädel, M., Steiner, J., Sumita, T., Takeyama, M., Tanaka, K., Toyoshima, A., Tsukada K., Türler, A., Usoltsev, I., Wakabayshi, Y., Wang, Y., Wiehl, N., Yamaki, S.: Synthesis and detection of a seaborgium carbonyl complex. Science **345**, 1491-1493 (2014)

[44] Kurz, N., Hoffmann, J., Minami, S., Ott, W.: The MBS Data Acquisition System for the Search of Element 120 at TASCA. GSI Scientific Report **PHN-IS-EE-02**, 252 (2011)

[45] Hoffmann, J., Kurz, N., Loechner, S., Minami, S., Ott, W., Rusanov, I., Voltz, S., Wieczorek, P.: New TASCA Data Acquisition Hardware Development for the Search of Element 119 and 120. GSI Scientific Report **PHN-IS-EE-03**, 253 (2011)

[46] Khuyagbaatar, J., Yakushev, A., Düllmann, Ch. E., Ackermann, D., Andersson, L. -L., Asai, M., Block, M., Boll, R. A., Brand, H., Cox, D. M., Dasgupata, M., Derkx, X., Di Nitto, A., Eberhardt, K., Even, J., Evers, M., Fahlander, C., Forsberg, U., Gates, J. M., Gharibyan, N., Golubev, P., Gregorich, K. E., Hamilton, J. H., Hartmann, W., Herzberg, R. -D., Heßberger, F. P., Hinde, D. J., Hoffmann, J., Hollinger, R., Hübner, A., Jäger, E., Kindler, B., Kratz, J. V., Krier, J., Kurz, N., Laatiaoui, M., Lahiri, S., Lommel, B., Maiti, M., Miernik, K., Minami, S., Mistry, A., Mokry, C., Omtvedt, J. P., Pang, G. K., Papadakis, P., Renisch, D., Roberto, J., Rudolph, D., Runke, J., Rykaczewski, K., Sarmiento, L. G., Schädel, M., Schausten, B., Semchenkov, A., Shaughnessy, D. A., Steinegger, P., Steiner, J., Tereshatov, E. E., Thörle-Pospiech, P., Tinschert, K., Torres De Heidenreich, T., Trautmann, N., Türler, A., Uusitalo, J., Ward, D. E., Wegrzecki, M., Wiehl, N., Van Cleve, S. M., Yakusheva, V.: ^{48}Ca + ^{249}Bk Fusion Reaction Leading to Element Z = 117: Long-Lived α-Decaying ^{270}Db and Discovery of ^{266}Lr. Phys. Rev. Lett. **112**, 172501-1- 172501-5 (2014)

[47] Khuyagbaatar, J., Yakushev, A., Düllmann, Ch. E., Ackermann, D., An-

dersson, L.-L., Block, M., Brand, H., Cox, D. M., Even, J., Forsberg, U., Golubev, P., Hartmann, W., Herzbzerg, R.-D., Heßberger, F. P., Hoffmann, J., Hübner, A., Jäger, E., Jeppsson, J., Kindler, B., Kratz, J. V., Krier, J., Kurz, N., Lommel, B., Maiti, M., Minami, S., Mistry, A. K., Mrosek, Ch. M., Pysmenetska, I., Rudolph, D., Sarmiento, L. G., Schaffner, H., Schädel, M., Schausten, B., Steiner, J., Torres De Heidenreich, T., Uusitalo, J., Wegrzecki, M., Wiehl, N., Yakusheva, V.: New Short-Lived Isotope ^{221}U and the Mass Surface Near N=126. Phys. Rev. Lett. **115**, 242502-1- 242502-5 (2015)

[48] Zvara, I.: Simulation of Thermochromatographic Processes by the Monte Carlo Method. Radiochimica Acta **38**, 95-101 (1985)

[49] Even, J., Yakushev, A., Düllmann, Ch. E., Dvorak, J., Eichler, R., Gothe, O., Hild, D., Jäger, E., Khuyagbaatar, J., Kratz, J. V., Krier, J., Niewisch, L., Nitsche, H., Pysmenetska, I., Schädel, M., Schausten, B., Türler, A., Wiehl, N., Wittwer, D.: Rapid Synthesis of Radioactive Transition-Metal Carbonyl Complex at Ambient Conditions. Inorg. Chem. **51**, 6431-6433 (2012)

[50] Lens, L., Yakushev, A., Düllmann, Ch. E., Asai, M., Ballof, J., Block, M., David, H. M., Despotopulos J., Di Nitto, A., Eberhardt, K., Even, J., Götz, M., Götz, S., Haba, H., Harkness-Brennan, L., Heßberger, F. P., Herzberg, R. -D., Hoffmann, J., Hübner, A., Jäger, E., Judson, D., Khuyagbaatar, J., Kindler, B., Komori, Y., Konki, J., Kratz, J. V., Krier, J., Kurz, N., Laatiaoui, M., Lahiri, S., Lommel, B., Maiti, M., Mistry, A. K., Mokry, C., Moody, K., Nagame, Y., Omtvedt, J. P., Papadakis, P., Pershina, V., Runke, J., Schädel, M., Scharrer, P., Sato, T., Shaughnessy, D., Schausten, B., Thörle-Pospiech, P., Trautmann, N., Tsukada, K., Uusitalo, J., Ward, A., Wegrzecki, M., Wiehl, N., Yakusheva, V.: To be submitted